

**Oxygen-Bearing Functionalities Enhancing NO<sub>2</sub>, NH<sub>3</sub>, and Acetone Electronic Response and Response Variation by Polythiophenes in Organic Field-Effect Transistor Sensors**

Journal:	<i>Journal of Materials Chemistry C</i>
Manuscript ID	TC-ART-09-2021-004650.R1
Article Type:	Paper
Date Submitted by the Author:	27-Dec-2021
Complete List of Authors:	Wagner, Justine; Johns Hopkins University Song, Yunjia; Johns Hopkins University, Materials Science and Engineering Shapiro, Jenna; Ann & Robert H Lurie Children's Hospital of Chicago Pritzker Department of Psychiatry and Behavioral Health Northwestern Univ Katz, Howard; Johns Hopkins University

# Oxygen-Bearing Functionalities Enhancing NO<sub>2</sub>, NH<sub>3</sub>, and Acetone Electronic Response and Response Variation by Polythiophenes in Organic Field-Effect Transistor Sensors

Justine Wagner<sup>a</sup>, Yunjia Song<sup>a</sup>, Jenna Shapiro<sup>b</sup>, and Howard E. Katz<sup>a\*</sup>

<sup>a</sup>Department of Materials Science and Engineering, Johns Hopkins University, 206 Maryland Hall, 3400 North Charles Street, Baltimore, MD 21218. <sup>b</sup>Ann & Robert H. Lurie Children's Hospital of Chicago, Pritzker Department of Psychiatry and Behavioral Health, Northwestern University Feinberg School of Medicine, Department of Psychiatry and Behavioral Sciences

\*Corresponding author: email [hekatz@jhu.edu](mailto:hekatz@jhu.edu)

**Abstract.** We investigated the enhanced vapor responses and altered response ratios of a series of thiophene (co)polymers with oxygenated side chains (CH<sub>2</sub>OH, linear polyethylene glycol, and crown ether), including the novel poly(3-hydroxymethylthiophene) (PTOH) and other newly synthesized polymers. Hydroxymethyl-containing copolymers had higher mobility compared to poly(3-hexylthiophene) (P3HT). The larger crown ether moiety promotes transistor characteristics of P3HT while the smaller one impairs them. Incorporating different oxygen bearing functionalities increased responses of thiophene polymers to NO<sub>2</sub>, NH<sub>3</sub>, and acetone. For example, a polyether side chain increases the NO<sub>2</sub> response sensitivity of copolymers of both P3HT and PTOH, but sensitivity towards gas analytes was more prominent for glycol-based functionalities rather than the crown ethers. PTOH is very sensitive to NO<sub>2</sub> and the response likely includes a contribution from conductive protons on the OH group. The lack of correlation among the rank-ordered gas sensitivities imparted by each functional group was found to be useful for designing a selective sensor array. We specifically showed high classification accuracy for all the polymer responses to NO<sub>2</sub> and acetone vapors, both of which

gave increased device currents but with response ratios different enough to allow highly classifying discriminant functions to be derived.

## 1. Introduction

Conducting polymers have received much attention for applications such as organic field-effect transistors (OFETs)<sup>1-2</sup>, light-emitting diodes<sup>3-6</sup>, sensor technology<sup>7-8</sup>, electrochromic devices<sup>9-11</sup>, supercapacitors<sup>12-13</sup>, organic solar cells<sup>14-15</sup>, and electromagnetic shielding<sup>16-17</sup>.

Regioregular polythiophenes (rr-PTs) have been regarded as promising for chemical sensors since they display fairly stable conductivity under ambient conditions, making them suitable for chemiresistive sensing. They are also soluble in a variety of organic solvents, their chemical composition may induce favorable and unique physical interactions between sensing materials and analytes, and they can be readily fine-tuned for analyte selectivity.<sup>18</sup>

Polar oxygen-containing functional groups on rr-PT side chains should increase noncovalent interactions between the polymers and polar vapor analytes, leading to increased electronic property changes induced by the analytes. There are already some reports of this occurring<sup>19-20</sup>, as will be pointed out later as well. However, there has been no broad, systematic study of polythiophene-based materials with specific terminal side chain functionalization affecting responses to vapors. In another class of electronic vapor-sensing materials, reduced graphene oxides (rGOs),<sup>21-28</sup> oxygenated functional groups led to improved sensitivity, enhanced response/recovery rates, and decreased detection limits. Oxygen-functional moieties consist of carbonyl, carboxyl, hydroxyl, and epoxy groups residing on the edge or basal plane depending on the functional moiety<sup>29</sup> and have demonstrated increased

responses to nitrogen dioxide ( $\text{NO}_2$ ) and ammonia ( $\text{NH}_3$ ).<sup>30-32</sup> Oxygen functional groups on graphene oxide or reduced graphene oxide are present as random arrangements of multiple functionalities that cannot easily be selectively produced or eliminated. Polythiophenes, on the other hand, have the advantage that the functional groups are incorporated individually during synthesis, allowing their individual effects on vapor responses to be determined.

A recent paper by Kang et al<sup>33</sup> seems to be the first to analyze the use of an additional type of oxygenated group, polyether chains, in a conjugated polymer system for vapor sensing, reporting -1.5%/ppm sensitivity to ammonia and 8000%/ppm sensitivity to  $\text{NO}_2$  from a branched polyethylene glycol (PEG) side chain on a high-mobility, weakly donating conjugated polymer backbone. They also indicated that alkyl side chains promoted carrier mobility while PEG side chains did not. Two earlier papers<sup>34-35</sup> demonstrated that graft copolymers with small amounts of PEG side chains improved sensor response due to their interaction with  $\text{NO}_2$ .

In our previous work<sup>36</sup>, we discovered that a polymeric thiophene carboxylic acid showed a dramatic and superlinear increase in drain current ( $I_D$ ) of over 15,000% to a ramped exposure of 10 ppm of  $\text{NO}_2$  while the corresponding response by its methyl ester was roughly 600% to a ramped exposure of 10 ppm  $\text{NO}_2$ . However, they both showed unconventional responses to  $\text{NH}_3$  with an increase in  $I_D$  to 200-300% from 10 ppm ramped  $\text{NH}_3$  exposure. That study showed two polar groups altering sensitivity to  $\text{NO}_2$  and interaction mechanisms with  $\text{NH}_3$  compared to alkyl chains such as poly(3-hexylthiophene) (P3HT).

Here, we report room-temperature responsiveness to nitrogen dioxide ( $\text{NO}_2$ ), ammonia ( $\text{NH}_3$ ), and acetone of polythiophene homopolymers and copolymers incorporating oxygenated functional group moieties ( $\text{CH}_2\text{OH}$ , linear PEG, and crown ether). While oxygenated moieties

can decrease the carrier mobility and alter the carrier concentration, sufficient conductivity is maintained for observing responses in chemiresistive or OFET modes. We study a new polythiophene-based polymer series consisting of copolymers of P3HT, and an additional novel homopolymer and copolymers incorporating the hydroxymethyl side chain, each with other oxygenated comonomers, which results in greatly increased polymer sensitivity to  $\text{NO}_2$  and altered ratios of the responses of the polymers to  $\text{NH}_3$  and acetone. We are able to match the sensitivity changes to the functional groups and obtain statistically distinguishable patterns of responses to the vapors allowing greatly increased selectivity among them.

## 2. Results

### A. Synthesis and Characterization of P3HT and P3HT copolymers

Figure 1 displays the structures of P3HT and P3HT copolymers. They were synthesized via

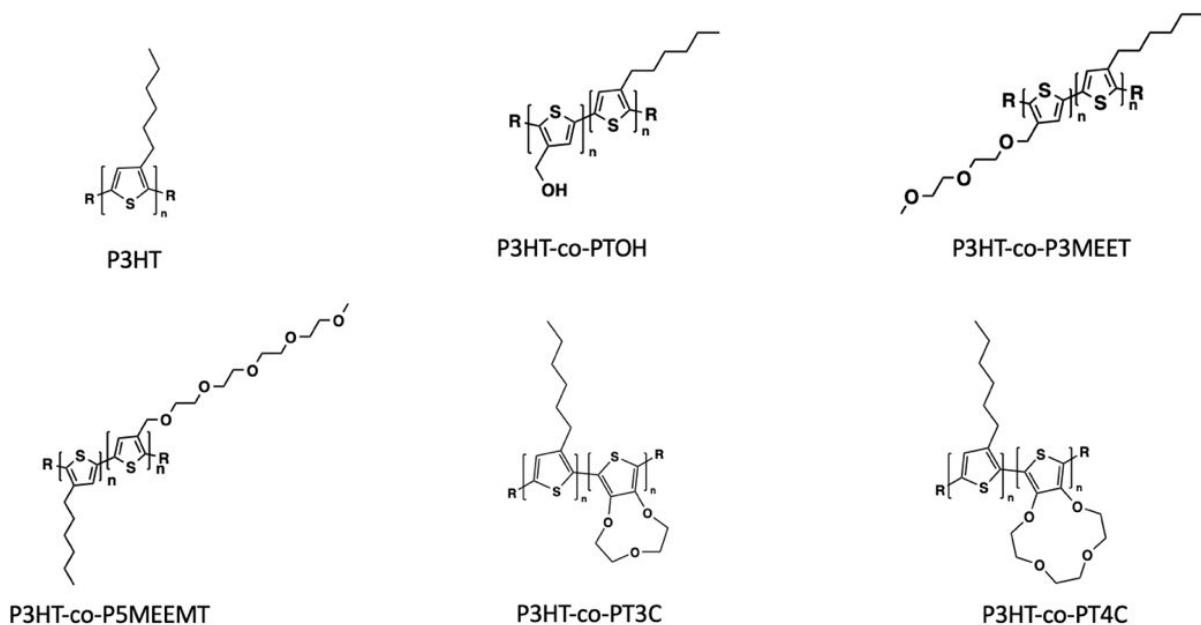


**Figure 1.** Molecular Structures of P3HT and P3HT-copolymers.

Kumada catalyst-transfer polycondensation (KCTP)/Grignard metathesis (GRIM) polymerization that gave high regioregularity.<sup>37-41</sup> Additional synthetic details are provided in Supporting Information. <sup>1</sup>H NMR and gel permeation chromatography (GPC) for these and the all-oxygenated copolymers discussed later are in Supporting Information, Figures S1-S33. Comonomer was added as 0.15 eq compared to 2,5-dibromo-3-hexylthiophene. It was intended that the polymers incorporate 10-25% of oxygen functionalized monomer unit as discussed in Supporting Information. P3HT-co-PTOH had 16% OH incorporation with >90% regioregularity, P3HT-co-P3MEEMT had 13% polyether incorporation with >88% regioregularity, P3HT-co-P5MEEMT had 14% polyether incorporation with >89% regioregularity, P3HT-co-PT3C had 25% crown incorporation with >87% regioregularity, and P3HT-co-PT4C had 20% crown incorporation with >88% regioregularity. GPC data are summarized in Table 1 and Supporting Information Figures S30-31. The polymers display similar molecular weight, polydispersity, and morphology, as summarized in the Supporting Information (page 35).

Table 1 GPC-reported molecular weight and polydispersity of P3HT and P3HT-co-polymers

Polymer	$M_n$	$M_w$	PDI
P3HT	10,988	16,162	1.5
P3HT-co-PTOH	11,421	15,965	1.4
P3HT-co-P3MEEMT	13,699	22,132	1.6
P3HT-co-P5MEEMT	11,110	16,239	1.5
P3HT-co-PT3C	11,207	18,035	1.6
P3HT-co-PT4C	12,373	20,545	1.7

## B. P3HT and P3HT-copolymer OFET Performance

The FET characteristics of the polymers were studied using a bottom-gate, top-contact device configuration. The polymers were deposited onto a p-doped silicon wafer with 300 nm of thermally grown silicon oxide. All polymers were deposited by spin-coating, interdigitated masks were placed on the polymers, and then vapor deposition of gold electrodes was done to form the source and drain.

Current-voltage ( $I_d$ - $V_g$ ) characteristic curves (transfer curves), of P3HT and P3HT-copolymers were measured under ambient conditions, with no intentional gas or light exposure, and are shown in Figure 2 A-E. P3HT analysis was conducted in our earlier work.<sup>36</sup> P3HT-co-PTOH showed increased drain current compared to P3HT-co-P3MEEMT, P3HT-co-P5MEEMT, P3HT-co-PT3C, and P3HT-co-PT4C, for which the increase in oxygen functionality decreases carrier mobility and mobile carrier concentration which results in low conductivity. This is expected, as multiple studies<sup>19,42-43</sup> reported lower mobility for alkoxy-substituted polythiophenes. This behavior could also be expected in crown-ether-functionalized polythiophenes; however, conformational differences<sup>44-45</sup> may cause the difference in OFET behavior between P3HT-co-PT3C (no gate voltage-dependent on-current) and P3HT-co-PT4C, where there is a slightly higher drain current and observable transfer behavior.

P3HT itself displays a drift under ambient conditions of -5% with 25 consecutive scans, while Figure 2 A-C shows that P3HT-co-PTOH, P3HT-co-P3MEEMT, and P35MEEMT show larger drift reaching 15-20% increases in drain current. Figure 2 D-E shows that P3HT-co-PT3C and P3HT-co-PT4C currents increase 38% and 35%, respectively. This may be induced by the crown ether cavity attracting guest species. Overall, incorporating oxygen

functionalization increases the tendency of ambient drift which may be the result of induced interaction with gas species including water vapor in the ambient air. In related work, we have developed circuit designs to compensate for this drift.<sup>46-47</sup> Also, as will be seen later, the responses to analyte vapors are generally far higher than the drift.

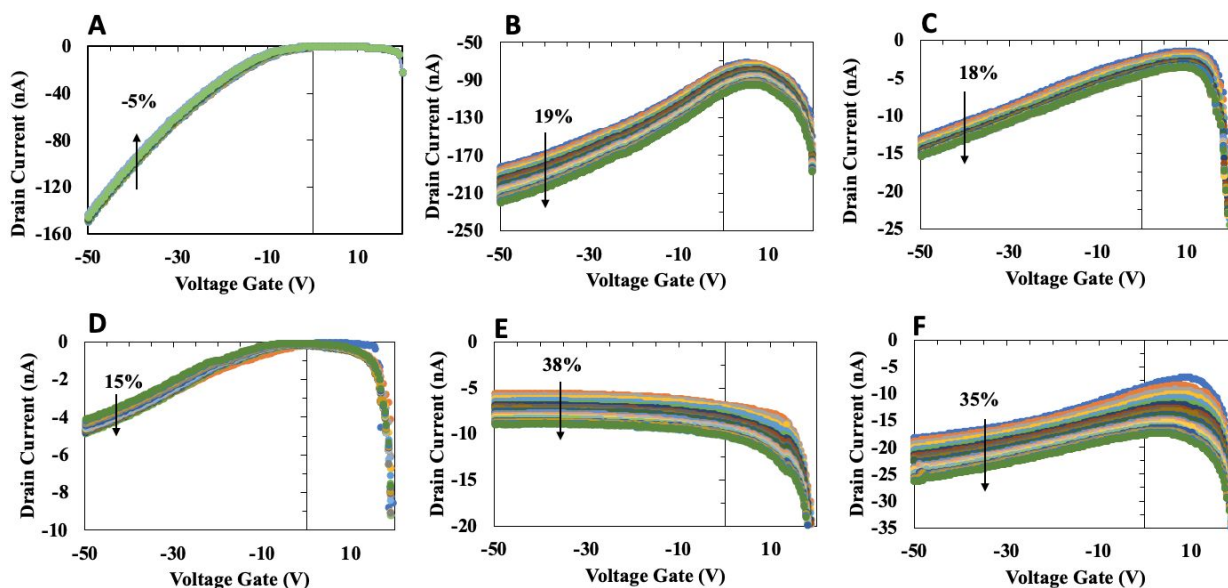


**Figure 2.** Transfer characteristics showing drift for polymers. (A) P3HT, (B) P3HT-co-PTOH, (C) P3HT-co-P3MEEMT, (D) P3HT-co-P5MEEMT, (E) P3HT-co-PT3C, and (F) P3HT-co-PT4C under ambient exposure condition and no light exposure. 25 consecutive scans were applied to analyze magnitude of drift as well as direction.

Figure 3 A-F displays the output characteristics under ambient conditions. P3HT exhibits typical p-channel behavior, while P3HT-co-PTOH and P3HT-co-PT3C display weak field effect transistor behavior. P3HT-co-PTOH also has a larger initial conductivity and off-current. P3HT-co-PT4C has a weak field effect transistor behavior as well; however, the incorporation of a 4-crown ether seems to restore the field effect characteristic behavior compared to the 3-crown counterpart. P3HT-co-P3MEEMT and P3HT-co-P5MEEMT also display p-channel behavior with a reduction of drain current as glycol chain length increases.

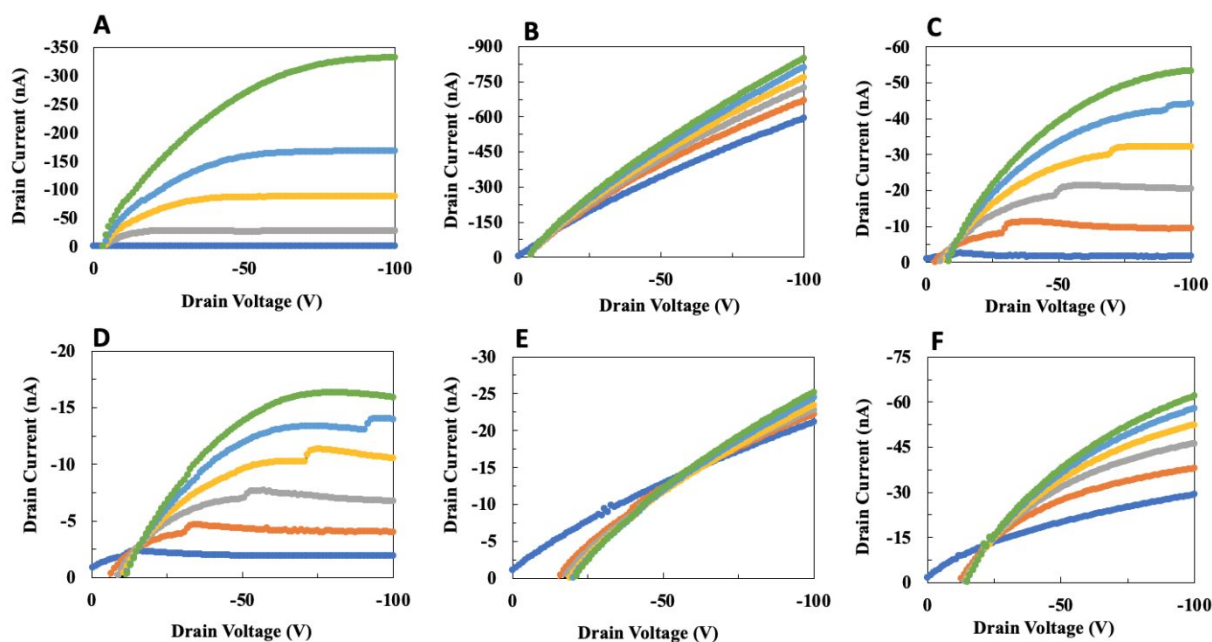


**Figure 3.** Output characteristic for polymer sensing layer (A)P3HT, (B) P3HT-co-PTOH, (C) P3HT-co-P3MEEMT, (D) P3HT-co-P5MEEMT, (E) P3HT-co-PT3C, and (F) P3HT-co-PT4C under ambient exposure condition, including no light exposure. An applied gate voltage of 0 to -100 V with a step size of -20 V was used.

### C. P3HT and P3HT Copolymer Responses to $\text{NO}_2$ and $\text{NH}_3$

Figure 4 A-F displays the output characteristics of the FETs with applied  $V_g = -50$  V on exposure to increasing concentrations of  $\text{NO}_2$  ranging from 0.5 ppm to 20 ppm. For tests of multiple concentration exposures, three minutes exposure time was permitted before transfer curves were measured, followed by the subsequent concentration. Four of each kind of sample were measured and averaged. Multiple plots on each graph correspond to different exposures, and the legend showing the gas concentrations is found on the right side of the figure.

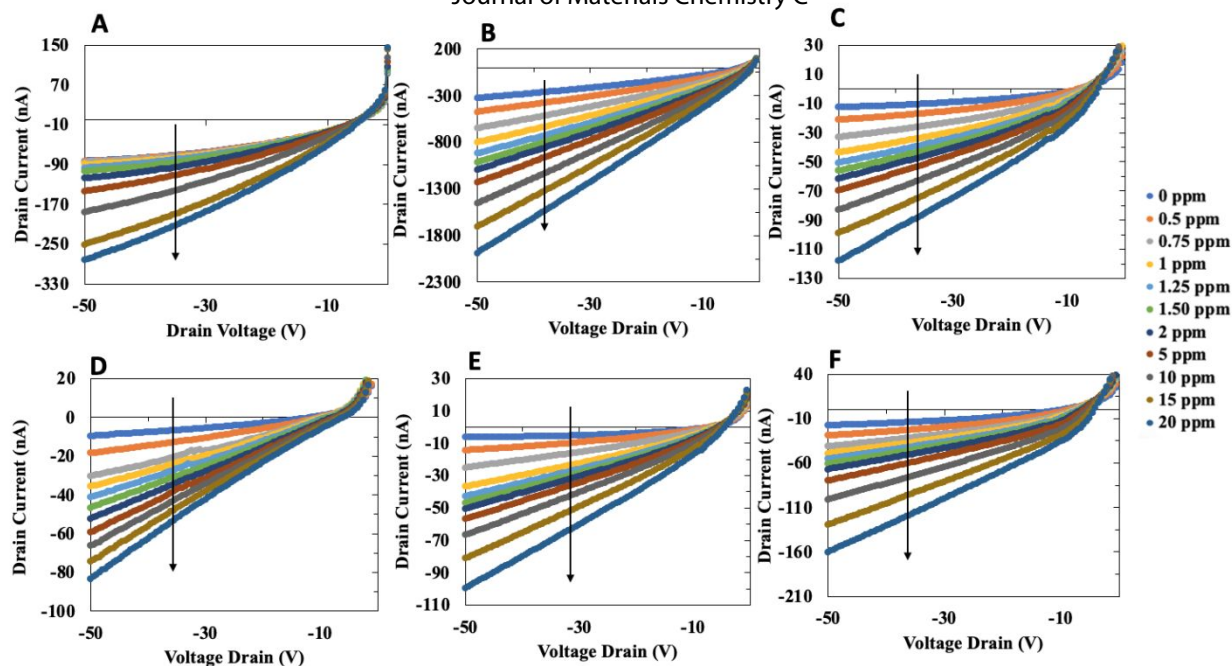


**Figure 4.** Output characteristic for polymer sensing layer (A) P3HT, (B) P3HT-co-PTOH, (C) P3HT-co-P3MEEMT, (D) P3HT-co-P5MEEMT, (E) P3HT-co-PT3C, and (F) P3HT-co-PT4C with continuous exposure to increasing concentrations of  $\text{NO}_2$  for 3 minutes before each consecutive measurement with an applied  $V_g = -50$  V. Concentrations are reported as volume ratios.

Transfer characteristics of the devices that correspond to the measured output characteristics are shown in in Figure S34, Supporting Information. Both output and transfer curves display expected response to  $\text{NO}_2$  where increased currents are observed for all five sets of copolymers with continued increase with each consecutive increasing concentration exposure. Therefore,  $\text{NO}_2$  displays continued conductance increases by  $\text{NO}_2$  induced p-doping.<sup>48</sup>

Figure 5 A-F displays the output characteristics of the FET-configured devices with an applied  $V_g = -50$  V on exposure to increasing concentrations of  $\text{NH}_3$  ranging from 0.5 ppm to 20 ppm. Transfer characteristics of the FETs pertaining to the measured output characteristics are shown in Figure S35, Supporting Information. All copolymers displayed typical p-type behavior with exposure to  $\text{NH}_3$ . This indicates that the general mechanism where  $\text{NH}_3$  causes a

decrease in  $I_D$  applies to these copolymers and indicates that the oxygen moieties do not substantially alter the carrier-quenching mechanism of interaction.

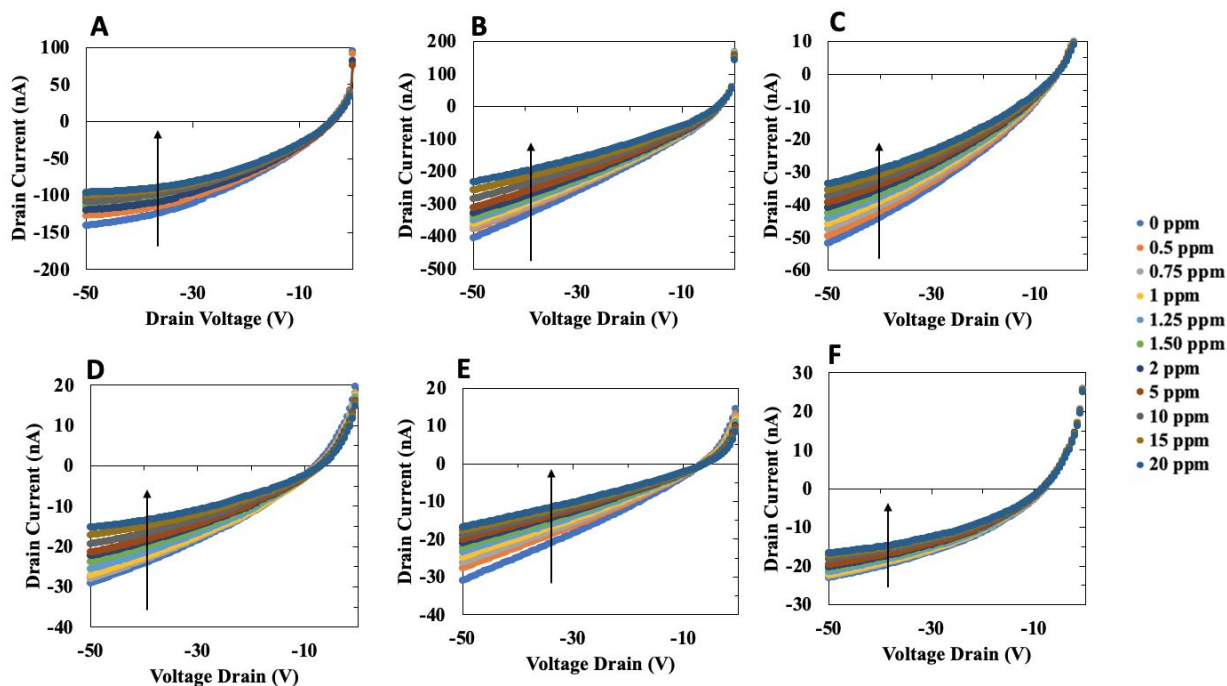


**Figure 5.** Output characteristic for polymer sensing layer A(A)P3HT, (B) P3HT-co-PTOH, (C) P3HT-co-P3MEEMT, (D) P3HT-co-P5MEEMT, (E) P3HT-co-PT3C, and (F) P3HT-co-PT4C with continuous exposure to increasing concentrations of  $\text{NH}_3$  for 3 minutes before each consecutive measurement with an applied  $V_g = -50$  V.

$\text{NH}_3$  is known to be a reducing gas analyte which decreases hole density, causing the observable decrease in  $I_D$  and  $\mu$ .<sup>49</sup>

The sensing capabilities of the polymers are quantified by extracting data from  $-50$  V bias voltage as shown in Figure 6. Figure 6A displays the response to continuous exposure to  $\text{NO}_2$  while Figure 6B displays the response to continuous exposure to  $\text{NH}_3$ . The sensitivity is calculated as the relative change in sensor current which is defined as:

$$S(\%) = \frac{I_{Gas} - I_{Air}}{I_{Air}} \times 100\%$$

where  $I_{Air}$  is the initial current before any target gas analyte is exposed to the polymer surface and measured in ambient air.  $I_{Gas}$  is the current under either  $NO_2$  or  $NH_3$  gas exposure. All copolymers show a general trend of cumulative response to  $NO_2$  in Figure 6A. P3HT-co-P5MEEMT showed the highest increase at about 1900% increase in  $I_D$ . P3HT, P3HT-co-PTOH, P3HT-co-P3MEEMT, P3HT-co-PT3C, and P3HT-co-PT4C reached a sensitivity of 260%, 600%, 800%, 900%, and 1000%, respectively. This demonstration of a crown substituent increasing vapor sensitivity is in contrast to an earlier report.<sup>50</sup> Regarding  $NH_3$  exposure (Figure 6B), as expected, a decrease in channel current was observed for all polymers where sensitivity was 30%, 40%, 46%, 50%, 50%, and 40% for P3HT, P3HT-co-PTOH, P3HT-co-P3MEEMT, P3HT-co-PT3C, and P3HT-co-PT4C, respectively. Assignment of the changes to mobility ( $\mu$ ) and threshold voltage ( $V_{TH}$ ) is in Supporting Information, Figures S36 and S37.

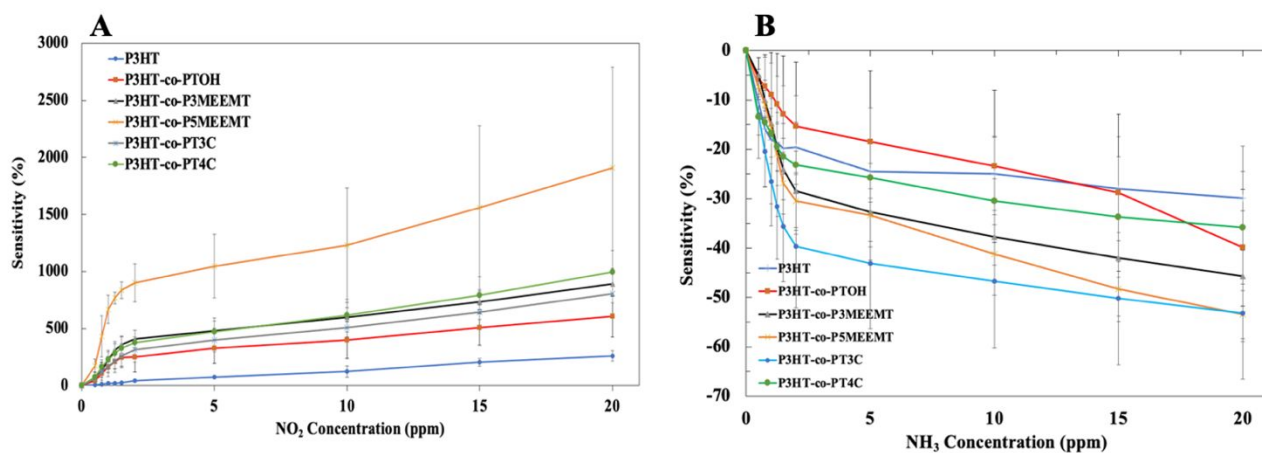


**Figure 6.** Sensitivity of each polymer sensing layer to various concentrations of (A)  $NO_2$  and (B)  $NH_3$  for 3 minutes before each consecutive measurement. This was repeated and averaged with at least 4 devices.

A continuous real-time transient response curve displaying the polymer response to 180 seconds of NO<sub>2</sub> exposure duration, followed by 12 minutes of recovery, and subsequent higher exposure from 0.5 ppm to 20 ppm is shown in Supporting Information Figure S38. After 20 ppm, a recovery period of 1 hour was evaluated for each polymer and shown in Supporting Information Figure S39. It appears that the incorporation of oxygen bearing functional groups results in a strong interaction that results in sluggish recovery under ambient conditions.

Using the same approach in our last work in extracting the limit of detection (LOD)<sup>36</sup>, P3HT-co-PTOH, P3HT-co-P3MEEMT, P3HT-co-P5MEEMT, P3HT-co-PT3C, and P3HT-co-PT4C display LOD of 270 ppb, 560 ppb, 280 ppb, 480 ppb, and 280 ppb, respectively for NO<sub>2</sub> exposure as shown in Supporting Information Figure S40. LOD for NH<sub>3</sub> exposure is shown in Figure S41.

These results so far show that incorporating oxygen bearing functionalities to the side chain of polythiophenes and forming a copolymer with pristine P3HT results in increasing the response sensitivity to NO<sub>2</sub> as well as towards NH<sub>3</sub> compared to pristine P3HT. This is consistent with the prior “branched PEG” study, where the larger PEG side chain resulted in the highest sensitivity.<sup>19-20,33</sup>

#### **D. Synthesis and Characterization of PTOH and PTOH- copolymers**

Figure 7 displays the molecular structures of PTOH and PTOH-copolymers. PTOH and PTOH-copolymers were synthesized via KCTP)/ (GRIM) as previously stated in Results Part A. <sup>1</sup>H NMR spectra are shown in Figures S20-29, Supporting Information. The formation of PTOTBS showed high degree of regioregularity at >95%. PTOH-co-P3MEEMT had 21% polyether incorporation with >70% regioregularity, PTOH-co-P5MEEMT had 15% polyether

incorporation with >68% regioregularity, PTOH-co-PT3C had 26% crown incorporation with >66% regioregularity, and PTOH-co-PT4C had 29% crown incorporation with >74% regioregularity. Incorporation of additional oxygen bearing moieties suppresses the regioregularity compared to PTOH itself.

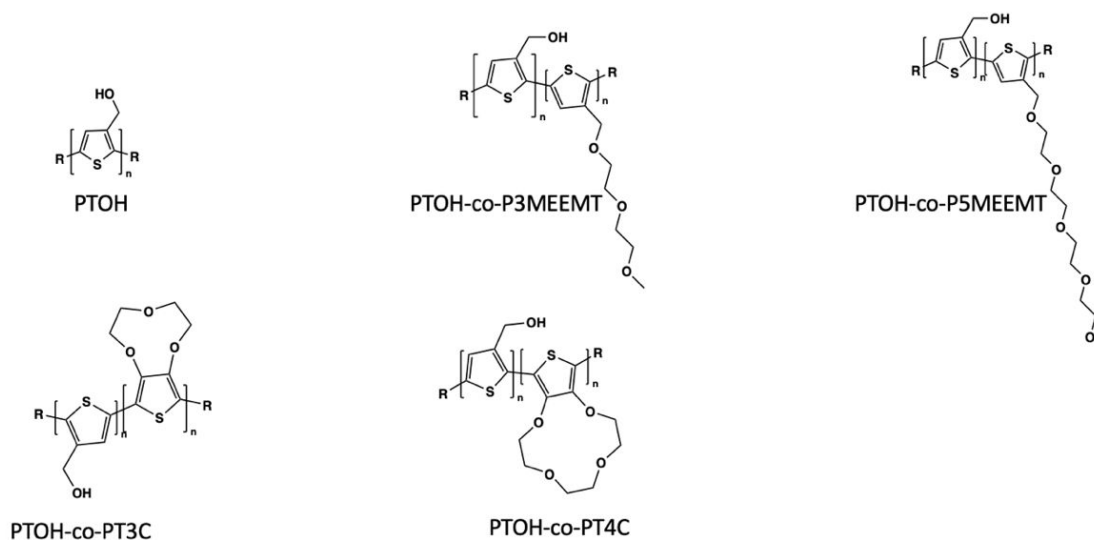


**Figure 7.** Molecular Structures of PTOH and PTOH-copolymers

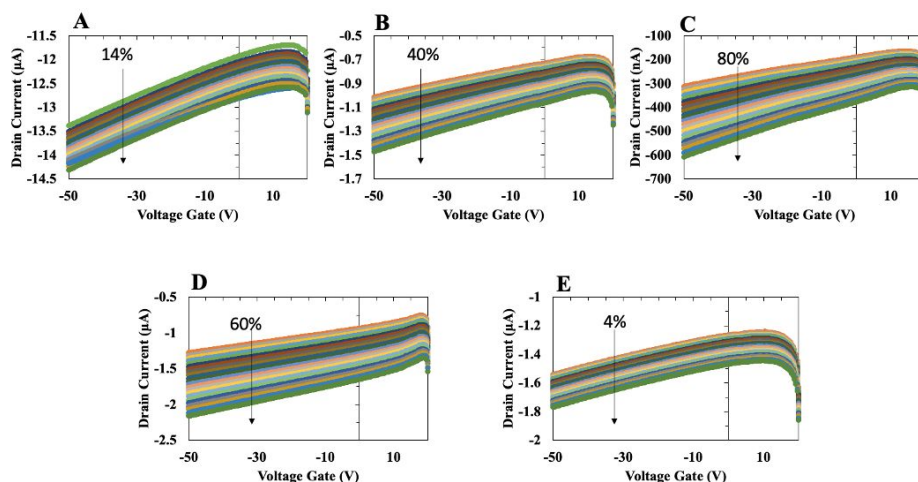
GPC data are shown in Table 2 and Supporting Information S32-33. The silyl protecting groups on the hydroxyl were used on GPC samples due to better solubility compared to the free hydroxylated polymers which require high polarity solvents such as DMF and higher temperature. The polymers show similar molecular weights and polydispersity.

Table 2 GPC-reported molecular weight and polydispersity of PTOH and PTOH copolymers.

Polymer	$M_n$	$M_w$	PDI
PTOTBS	7,073	11,618	1.6
PTOTBS-co-P3MEEMT	7,026	11,193	1.6
PTOTBS-co-P5MEEMT	6,673	11,300	1.7
PTOTBS-co-PT3C	5,372	9,025	1.7
PTOTBS-co-PT4C	7,973	15,039	1.9

### E. PTOH and PTOH copolymer OFET Performance

The FET characteristics of the polymers were studied using a bottom-gate, top-contact device configuration. Transfer curves of PTOH and PTOH-copolymers were measured under ambient conditions, with no intentional gas or light exposure, and are shown in Figure 8 A-E.



**Figure 8.** Transfer curves showing drifts for polymers. A) PTOH, (B) PTOH-co-P3MEEMT, (C) PTOH-co-P5MEEMT, (D) PTOH-co-PT3C, and (E) PTOH-co-PT4C under ambient conditions.

PTOH displayed the highest drain current, reaching tens of  $\mu\text{A}$  (though much of this is off current) while the rest of the copolymers show lower  $\mu$  and charge carrier density, resulting in lower drain current, which implies that the all-hydroxyl environment is different compared to that with the other oxygen bearing moieties. PTOH itself displays an ambient drift of  $13 \pm 7\%$  with 25 consecutive scans, while Figure 8 B-E shows that PTOH-co-P3MEEMT, PTOH-co-

P5MEEMT, PTOH-co-PT3C, and PT4C show more drift reaching  $54 \pm 9\%$ ,  $100 \pm 10\%$ ,  $61 \pm 30\%$ , and  $21 \pm 5\%$ , respectively. PTOH-co-PT4C surprisingly displays less drift.

Figure 9 A-E displays the output characteristics under ambient conditions. This time it can be clearly seen that PTOH, and all copolymers display weak field effect transistor behavior starting from 0 gate volts. PTOH-co-P3MEEMT, PTOH-co-P5MEEMT, and PTOH-co-PT3C appear to have a slightly stronger field effect transient behavior compared to PTOH and PTOH-co-PT4C. This behavior was observed in our previous work<sup>36</sup> for PTCOOH, and it is possible that the proton of the hydroxyl group participates in a self-doping mechanism which may weaken the field effect transistor behavior.<sup>51-53</sup>

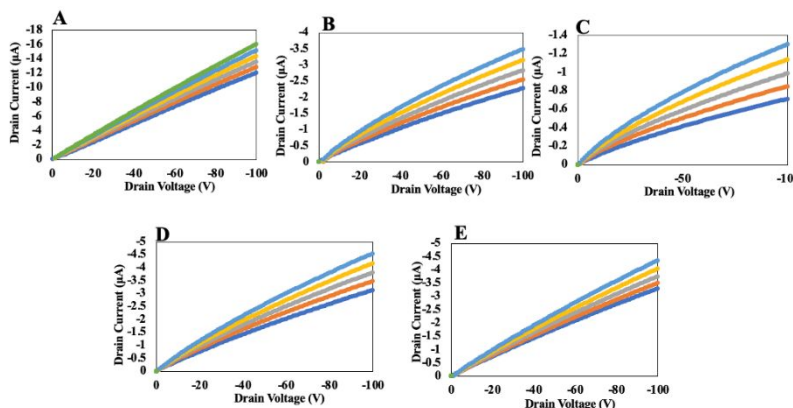


**Figure 9.** Output characteristics for polymers A) PTOH, (B) PTOH-co-P3MEEMT, (C) PTOH-co-P5MEEMT, (D) PTOH-co-PT3C, and (E) PTOH-co-PT4C under ambient conditions. An applied gate voltage of 0 to -100 V with a step size of -20 V was set.

### F. PTOH and PTOH copolymer Sensing Response to NO<sub>2</sub> and NH<sub>3</sub>

Figure 10 A-E shows output characteristics of the FET-configured devices with an applied  $V_g = -50$  V upon exposure to increasing concentrations of NO<sub>2</sub> that ranges from 0.5 ppm to 20 ppm. LOD determinations are shown in Figure S41, Supporting information. The corresponding transfer characteristics are shown in Figure S42, Supporting Information.

Again, both output and transfer curves display very strong responses to  $\text{NO}_2$  in the expected current-increase direction.

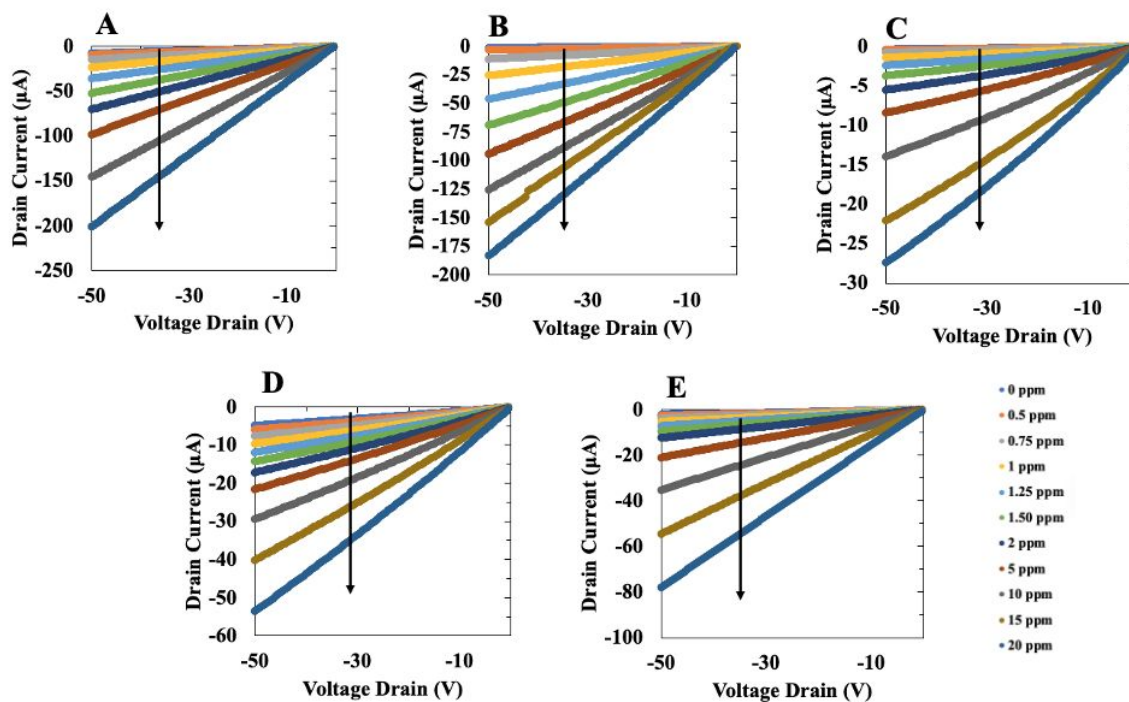


**Figure 10.** Output characteristic for polymer sensing layer A) PTOH, (B) PTOH-co-P3MEEMT, (C) PTOH-co-P5MEEMT, (D) PTOH-co-PT3C, and (E) PTOH-co-PT4C with continuous exposure to increasing concentrations of  $\text{NO}_2$  for 3 minutes before each consecutive measurement with an applied  $V_g = -50$  V.

Figure 11 A-E displays the output characteristic of the FET-configured devices with an applied  $V_g = -50$  V upon exposure to increasing concentrations of  $\text{NH}_3$  ranging from 0.5 ppm to 20 ppm.

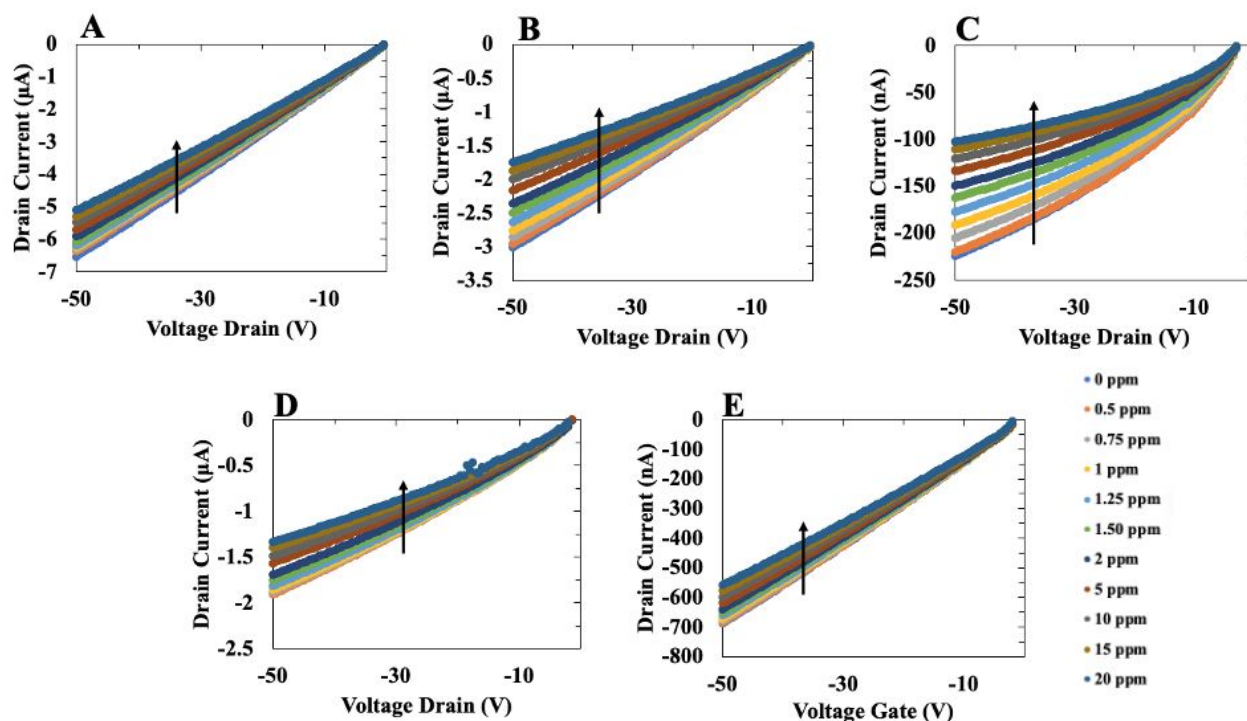


**Figure 11.** Output characteristic for polymer sensing layer A) PTOH, (B) PTOH-co-P3MEEMT, (C) PTOH-co-P5MEEMT, (D) PTOH-co-PT3C, and (E) PTOH-co-PT4C with continuous exposure to increasing concentrations of  $\text{NH}_3$  for 3 minutes before each consecutive measurement with an applied  $V_g = -50$  V.

Transfer characteristics of the FETs pertaining to the measured output characteristics are shown in Figure S43, Supporting Information. All copolymers displayed typical p-type behavior with exposure to  $\text{NH}_3$ . This again proves that the general mechanism where  $\text{NH}_3$  decreases the flow of current in the channel resulting in the decrease in  $I_D$  still applies, in contrast to our previous study where PTCOOH and PTCOOR displayed an unconventional, current-increase response to  $\text{NH}_3$ .

Supporting Information Figure S44 A-E displays  $\mu$  and  $V_{\text{TH}}$  shift extracted from the transfer curve of each consecutive increasing concentration exposure of  $\text{NO}_2$  to each polymer system. PTOH itself displays the highest  $\mu$  with no gas exposure at  $1.14 \times 10^{-2} \text{ cm}^2\text{V}^{-1}\text{s}^{-1}$ . We

noted above that P3HT-co-PTOH displayed a high  $\mu$  as well compared to pristine P3HT and the other co-polymers.  $\mu$  and  $V_{TH}$  shift extracted from the transfer curve of each consecutive increasing concentration exposure of  $NH_3$  to each polymer system are shown in Supporting Information, Figure S45 A-E.

Figure 12A displays the response to continuous exposure to  $NO_2$  while Figure 12B displays the response to continuous exposure to  $NH_3$ . The sensitivity was again calculated using the relative change in sensor current as defined earlier.

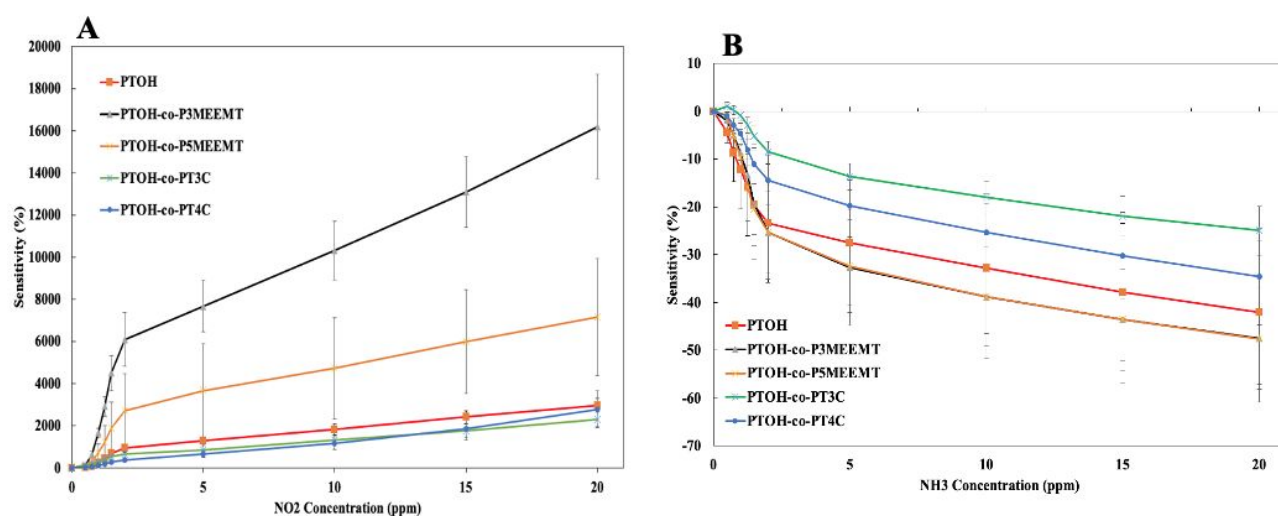


**Figure 12.** Sensitivity response of each polymer sensing layer to various concentrations of (A)  $NO_2$  and (B)  $NH_3$  for 3 minutes before each consecutive measurement. This was repeated and averaged with at least 4 devices.

All the PTOH and PTOH based co-polymers show a general trend of cumulative response to  $NO_2$ . PTOH-co-P3MEEMT showed the highest increase at about 16,000% increase in  $I_D$ . PTOH, PTOH-co-P5MEEMT, PTOH-co-PT3C, and PTOH-co-PT4C reached a sensitivity of 3000%, 7200%, 2800%, and 2300%, respectively. PTOH homopolymer showed about the same sensitivity as had the PEG-P3HT copolymer discussed earlier and much higher than that

of P3HT, while PTOH-co-P3MEEMT had sensitivity almost as high as the branched PEG copolymer reported earlier.<sup>33</sup> Thus, a clear synergy between the OH and shorter PEG group was demonstrated. Regarding NH<sub>3</sub> exposure (Figure 12B), as expected, a decrease in channel current was observed for all polymers where sensitivity decreased a maximum by 42%, 48%, 48%, 50%, 25%, and 35 % for PTOH, PTOH-co-P3MEEMT, PTOH-co-P5MEEMT, PTOH-co-PT3C, and PTOH-co-PT4C, respectively.

A continuous real-time transient response curve displaying polymer responses to 180 seconds of NO<sub>2</sub> exposure from 0.5 ppm to 20 ppm followed by 12 minutes of recovery is shown in Supporting Information Figure S46. The recoveries are shown in Supporting Information Figure S47.

In our previous work,<sup>36</sup> the LOD was extracted as the concentration where the measurement would equal the sample blank (after stabilization) plus the standard deviation of the analyte signal at the lowest measured concentration. However, PTOH-co-PT3C is the only polymer out of the present subset that displays linear response to NO<sub>2</sub> exposure. PTOH, PTOH-co-P3MEEMT, PTOH-co-P5MEEMT, PTOH-co-PT3C, and PTOH-co-PT4C required power functions of concentration to calculate LODs, which were LOD of 550 ppb, 500 ppb, 650 ppb, 1.3 ppm, and 650 ppb, respectively for NO<sub>2</sub> exposure, as shown in Supporting Information Figure S48. Unlike with the trend discovered with P3HT and P3HT based copolymers, the incorporation of additional oxygen bearing moieties worsens the LOD while only P3MEEMT shows slight improvement in the LOD. PTOH and most of the copolymers display a third order response while P3HT and P3HT based copolymers display a first-order response. This suggests that, just like reported previously for PT-COOH,<sup>36</sup> an effect where NO<sub>2</sub>

is simultaneously increases the hole transport and transport of protons is observed. The same principle was used to find the LOD for  $\text{NH}_3$  exposure, which was 497 ppb, 636 ppb, 112 ppb, 372 ppb and 198 ppb, respectively and shown in Supporting Information Figure S49. The LOD was reduced to a certain extent by incorporating oxygen bearing moieties for each subset of copolymers compared to PTOH except for PTOH-co-P3MEEMT.

### F. Remote gate (RG) Platform to elucidate $\text{NO}_2$ gas response mechanism of PTOH

In a recent publication<sup>54</sup>, we had developed a way to measure changes to the surface potential of the polymer film using a remote-gate field transistor (RG FET) in which the polymer is coupled to the oxide gate of the commercial silicon FET. In another recent study, we used the platform to measure the surface interaction of PTCOOH to understand the unusual high response this polymer had to  $\text{NO}_2$ .<sup>36</sup> As discussed above, PTOH has a very large response to  $\text{NO}_2$  with a response of 3000% after 20 ppm exposure and it displays a third-order interaction with  $\text{NO}_2$ . We further employ the RG FET platform to calculate the hole concentration, mobility, and conductivity and update our previous results that now include PTOH data in Figure 13.

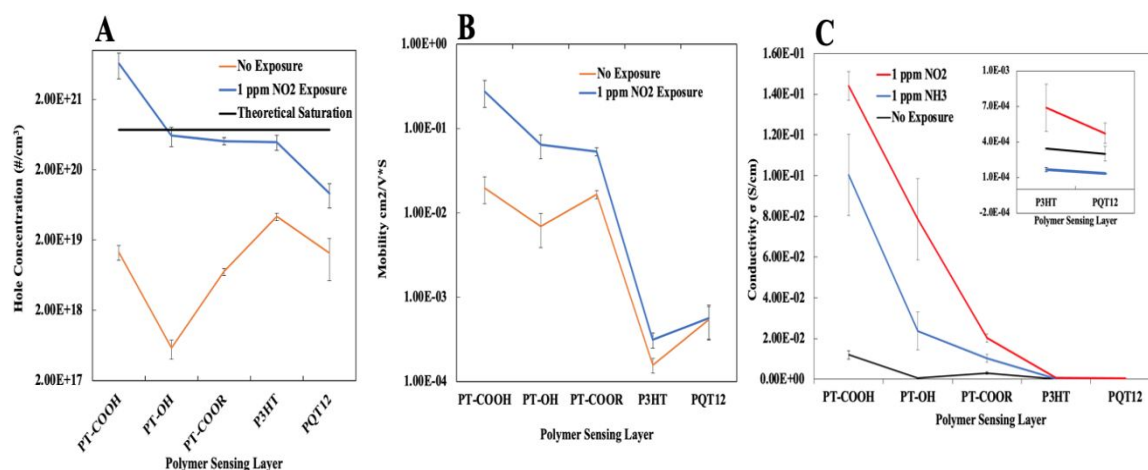


**Figure 13.** (A) Hole concentrations of polymer sensing layer before and after 1 ppm of NO<sub>2</sub> due to calculating the voltage shift occurrence with the incorporation of the RG FET platform. Initial hole concentration was obtained from  $\mu_h$  from OFET using transfer curve and conductivity ( $\sigma$ ). (B) Mobility for unexposed device was obtained from FET measurements, while mobility for NO<sub>2</sub>-exposed devices was calculated based on hole concentrations obtained by using  $\sigma = e \cdot \mu_h \cdot p_0$ . (C) Conductivity measurement of polymer sensing layer before and after 1 ppm NO<sub>2</sub> and NH<sub>3</sub> exposure.

Supporting Information Figure S50 displays the transfer curve of the RG FET system for PTOH as well as the visualization of the  $V_{TH}$  shift with exposure to NO<sub>2</sub>. In addition, Table S1 summarizing the electrical parameters extracted from the RG FET are shown in Supporting Information. It is observed that PTOH has an apparent hole concentration that reaches or is at the borderline value of the theoretical charge carrier density saturation magnitude that a polythiophene polymer can attain. We had reported that PTCOOH exceeds this theoretical charge density saturation value because of the conductive protons on the carboxylic acid that results in adding a generated positive current to the hole current flow through the polymer main chains. It seems that the much less acidic hydroxyl group proton must also be contributing additional positive current with NO<sub>2</sub> exposure.

### G. Acetone Sensitivity & Data Analysis

Acetone vapor can be used to diagnose diabetes, glucose-related dysregulation, or lung cancer through the exhaled breath.<sup>55-56</sup> Breath acetone concentration (BrAce) is measured in exhaled breath to monitor ketosis in healthy and diabetic subjects, providing an attractive alternative compared to other fluid analysis pathways.<sup>57</sup> To determine the sensitivity and selectivity of P3HT-copolymers and PTOH-copolymers towards acetone, each was analyzed

for differential sensing performance with the incorporation of oxygen functionalization, as shown in Figure 14.

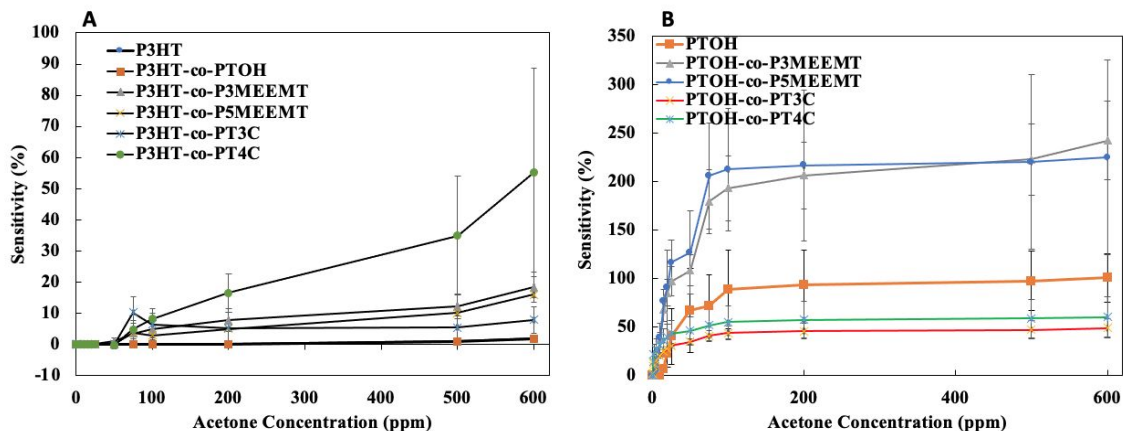


**Figure 14.** Sensitivity of each polymer sensing layer to various concentrations of acetone for (A) P3HT-copolymers and (B) PTOH-copolymers for 3 minutes before each consecutive measurement. This was repeated and averaged with at least 4 devices.

According to Figure 14A, P3HT displays no significant response to acetone. It is not until about 500-600 ppm where a slight increase in current is observed. P3HT-co-PTOH overlays P3HT and displays the same response. P3HT-co-PT4C displays a significant response to acetone and is improved compared to P3HT alone by having an onset of response by about 50 ppm of acetone and reaching about 55% sensitivity by 600 ppm. In Figure 14B, PTOH alone shows a larger response to acetone than P3HT and displays an onset in response of about 10 ppm of acetone, reaching about 50% increase in sensitivity at 600 ppm. Incorporating linear glycol chains increased the sensitivity of PTOH to acetone by 4-fold.

Supporting Information Figure S51-52 shows the  $\mu$  and  $V_{TH}$  shift extracted from the transfer curve of each consecutive increasing concentration exposure of acetone to each polymer system. The change in  $\mu$  differs slightly after running through all consecutive increasing acetone concentrations of P3HT based copolymers.  $\mu$  changes by 26%, -14%, 29%, 6.3%, 43%, and

60.5% for P3HT, P3HT-co-PTOH, P3HT-co-P3MEEMT, P3HT-co-P5MEEMT, PTOH-co-PT3C, and PTOH-co-PT4C, respectively.  $V_{TH}$  for P3HT, P3HT-co-PTOH, P3HT-co-P3MEEMT, P3HT-co-P5MEEMT, PTOH-co-PT3C, and PTOH-co-PT4C changes by -71%, 3.3%, 3.8%, 33%, -1.3%, and -12.5%, respectively. For PTOH based copolymers  $\mu$  changes by 70%, 190%, 220%, 63%, and 26% for PTOH, PTOH-co-P3MEEMT, PTOH-co-P5MEEMT, PTOH-co-PT3C, and PTOH-co-PT4C, respectively.  $V_{TH}$  shifts positively for all at 6.5%, 6.5%, 26%, 12%, and 7.5% for PTOH, PTOH-co-P3MEEMT, PTOH-co-P5MEEMT, PTOH-co-PT3C, and PTOH-co-PT4C, respectively. Cavallari et al<sup>55</sup> reported for a P3HT OFET that at 40 nm thickness, P3HT displays an increase in current of  $40 \times 10^{-4} \%$  /ppm, nearly doubling to  $75 \times 10^{-4} \%$  /ppm at 80 nm thickness.  $\mu$  and  $V_{TH}$  also increase for a 40 nm film by  $22 \times 10^{-4} \%$  /ppm and  $20 \times 10^{-4} \%$  /ppm, respectively. They indicate that P3HT films have both crystalline and amorphous phases and the gaseous analyte may induce changes on the crystal lattice parameters that may affect charge hopping or affect charge trapping. They concluded that the adsorption of acetone on P3HT thin films reduces the average spacing among polymer molecules by induced Van der Waals force, therefore increasing  $\pi$ -molecular orbital stacking and thin-film conductivity. Since our work involves poly(alkylthiophene)-based systems, we hypothesize that the work of Cavallari (mentioned in the paragraph above and present as reference 55) is particularly relevant, with an analogous response mechanism.

In another report by Bertoni et al<sup>58</sup>, P3HT nanofibers showed an increase in current with acetone and a sensitivity of about 3.5% at 17.6 ppm of acetone exposure. Acetone was reported to be capable of altering resistance of the polymeric film by altering the intermolecular packing.<sup>55,58</sup>

A linear discriminant analysis<sup>59-60</sup> was conducted using response data from all eleven polymers, plus poly(thiophene-3-butyric acid) and its methyl ester characterized previously<sup>36</sup> to differentiate NO<sub>2</sub> versus acetone, both of which induced current-increase responses from all the polymers. All the tested concentrations of NO<sub>2</sub> (0.5ppm, 1ppm, 2ppm, 5ppm) and acetone (20ppm, 50ppm, 100ppm, 200ppm, 500ppm) were included. The set of polymers significantly predicted volatile type: Wilk's  $\Lambda=0.03$  (can range from 0 to 1; 0 is perfect discrimination;  $\chi^2(13) = 97.41$  (higher values mean greater discrimination);  $p < .001$ , with essentially 100% accuracy. The standardized canonical discriminant function coefficients for each polymer indicated that the polymers that most strongly discriminated between NO<sub>2</sub> and acetone were P3HT-co-P3MEEMT (18.36), PTOH-co-PT3c (17.87), P3HT-co-PTOH (-14.44), PTCOOH (-14.10), and P3HT (11.52).

A second linear discriminant analysis was performed, again on all thirteen polymers, but this time using only the smallest tested concentrations of NO<sub>2</sub> (0.5ppm) and acetone (20ppm). The polymers again significantly predicted volatile type,  $\Lambda=0.01$ ,  $\chi^2(6) = 13.94$ ,  $p=0.030$ , with essentially 100% accuracy. The standardized canonical discriminant function coefficients for each polymer indicated that the polymers that most strongly discriminated between NO<sub>2</sub> and acetone were PTOH-co-P5MEEMT (4.53), PTOH-co-P3MEEMT (-4.12), P3HT (-4.21), PTOH (2.62), PTOH-co-PT3c (2.12), and PTOH-co-PT4c (2.03). When comparing NO<sub>2</sub> (0.5ppm) with each of the other higher acetone concentrations, the set of polymers again predicted volatile type with 100% classification accuracy. This indicates that even in the response ranges where absolute signals from the two gases would overlap, the different ratios among the responses provided considerable selectivity. Furthermore, the novel PTOH-containing polymers of this proposal provided the greatest fractional contributions to the discrimination.

Although  $\text{NH}_3$  can be trivially distinguished from the other two vapors because it generally induces current-decrease responses, it was included in an additional linear discriminant analysis to provide a means of visualizing the discrimination. Two discriminant functions were evaluated given that there were three volatile types. Both functions had in a significant association between groups and predictors, (discriminant function 1 and 2 combined,  $\Lambda=.02$ ,  $\chi^2(26) = 196.77$ ,  $p < .001$ , discriminant function 2,  $\Lambda=.20$ ,  $\chi^2(12) = 75.75$ ,  $p < .001$ ), indicating that both functions significantly accounted for the relationship between polymers and volatile type. The first discriminant function expressed most of the between-group variability in volatile type (75.1%, canonical  $R^2 = .96$ ) and the second discriminant function accounted for 24.9% of the between-group variability (canonical  $R^2 = .90$ ). Response data mapped along the two discriminant functions are shown in Figure 15.

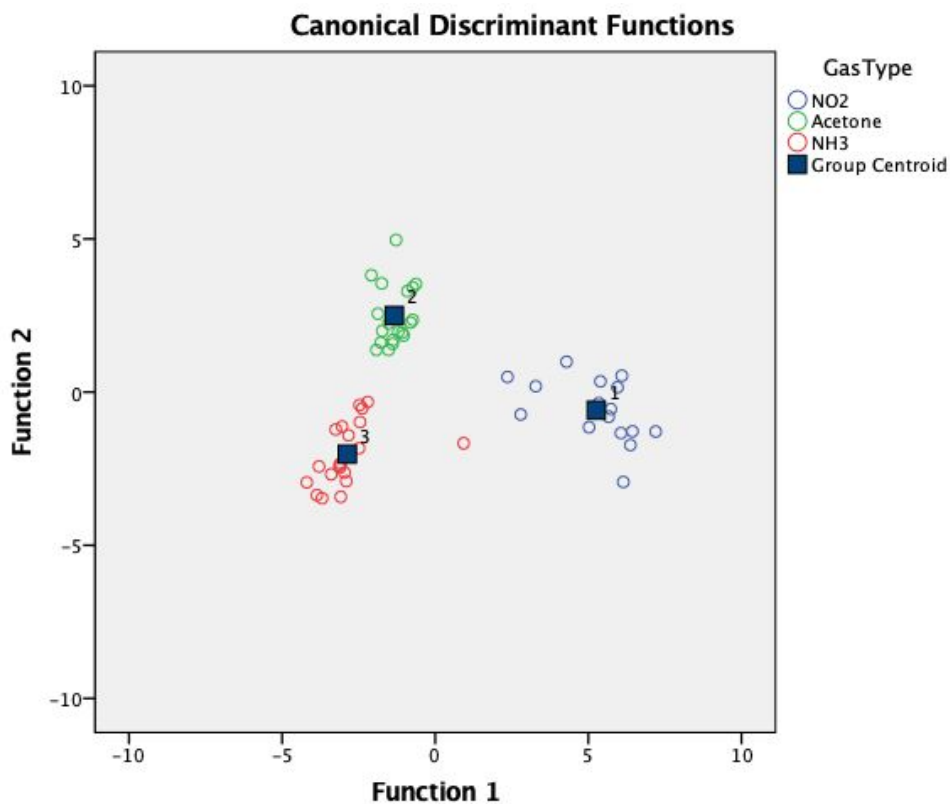


**Figure 15.** Response data for each vapor converted to coordinates along two discriminant functions.

The first discriminant function maximally separates  $\text{NO}_2$  from acetone and  $\text{NH}_3$ . The second discriminant function separates acetone from  $\text{NH}_3$  and provides some further separation between acetone and  $\text{NO}_2$ . PTOH-co-PT3c, P3HT-co-P3MEEMT, and P3HT have high loadings on the first discriminant function, indicating that the combination of these polymers mostly strongly distinguishes  $\text{NO}_2$  from the other two volatiles. PTOH-co-PT4c and PTOH-co-P5MEEMT load highly on the second discriminant function, which most strongly distinguishes acetone from the other two volatiles. The set of predictors was 100% accurate in classifying volatile type. This indicates that the set polymers are able to significantly distinguish among  $\text{NO}_2$ , acetone, and  $\text{NH}_3$ .

To fully summarize the gas sensing performance of all sets of polymers that were designed, Supporting Information Figure S53 displays the sensitivity of all the polymers to each gas exposure using gas concentration of % / ppm. P3HT-co-P5MEEMT (S53A) displays the highest sensitivity at 95 % / ppm for  $\text{NO}_2$  induced exposure while PTOH-co-P3MEEMT (S53B) displays an exceptionally high sensitivity of 810 % / ppm. Regarding acetone exposure, P3HT-co-PT4C displayed a high sensitivity of 92 % / ppm while PTOH-co-P3MEEMT and PTOH-co-P5MEEMT were comparable with record high sensitivity of 375 and 400 % / ppm, respectively. Regarding  $\text{NH}_3$  exposure, the crown ethers of P3HT-co-PT3C and P3HT-co-PT4C were comparable, reaching -2.5 % / ppm while PTOH-co-P3MEEMT and PTOH-co-P5MEEMT were comparable, reaching -2.4 % / ppm.

### 3. Summary and Conclusions

Various new thiophene (co) polymers incorporating oxygenated functional groups were synthesized. Incorporating different oxygen bearing functionalities increases responses of thiophene polymers to  $\text{NO}_2$ ,  $\text{NH}_3$ , and acetone. A polyether side chain increases the  $\text{NO}_2$  response sensitivity of copolymers of both P3HT and PTOH. However, sensitivity towards gas analytes was more prominent for glycol-based functionalities rather than the porous crown ethers. In comparing device performance, PTOH and PTOH-based copolymers had higher initial  $\mu$  compared to P3HT, with substantial off current as well. It is interesting to note that the larger crown ether moiety promotes transistor characteristics of P3HT while the smaller one impairs them.

PTOH itself is very sensitive to  $\text{NO}_2$  due partly to conductive protons on the hydroxyl group that can add positive current to the hole current flow through the polymer main chains. This study and our previous study<sup>35</sup> demonstrate that carboxyl groups add the most sensitivity to  $\text{NO}_2$  with hydroxyl next. It is further confirmed that even though hydroxyls confer a stronger response to  $\text{NO}_2$  compared to alkyl chain moieties such as P3HT, the recovery of OH polymers is sluggish and would require additional energetic input to eject the  $\text{NO}_2$  gas molecules to restore the initial film conditions.

One final important conclusion is that the lack of correlation among the rank-ordered gas sensitivities imparted by each functional group is useful for designing selective sensor arrays with a minimum number of circuit elements. We specifically showed high classification accuracy for all the polymer responses to  $\text{NO}_2$  and acetone vapors, both of which gave increased device currents but with response ratios different enough to allow highly classifying discriminant functions to be derived.

#### 4. Acknowledgments, Conflict of Interest Statement, and Author Contributions

We thank the National Science Foundation, grant numbers ECCS 1807293 (organic transistor and vapor exposure studies) and DMR 1807292 (RG investigations) for funding. The authors also would like to thank Professor Rebekka Klausen (Johns Hopkins University) and Yuyang Ji for use of the GPC facility. We gratefully acknowledge the assistance of Nan (Louise) Chen with thickness measurements, and Dr. Patty McGuiggan for AFM.

The authors declare no conflicts of interest. All experimental work (synthesis, characterization, device and response testing) was performed and drafted by Dr. Wagner. The morphology study was done by Ms. Song. The statistical analysis was carried out and written by Dr. Shapiro. The project was constructed and planned, and the manuscript organized and edited, by Prof. Katz.

#### 5. References

- 1) Yawson, B.N.; Noh, Y.Y. Organic Thin Film Transistor with Conjugated Polymers for Highly Sensitive Gas Sensors. *Macromolecular Research*. **2017**, 25 (6), 489-495.  
<https://doi.org/10.1007/s13233-017-5108-7>
- 2) Yan, H.; Chen, Z.; Zheng, Y.; Newman, C.; Quinn, J.R.; Dotz, F.; Kastler, M.; Facchetti, A. A High-Mobility Electron-Transporting Polymer for Printed Transistors. *Nature*. **2009**, 457 (7230), 679-86. <https://doi.org/10.1038/nature07727>
- 3) Perepichka, I.F.; Perepichka, D.F.; Meng, H.; Wudl, F. Light-Emitting Polythiophenes. *Adv. Mater.* **2005**, 17, 2281-2305. <https://doi.org/10.1002/adma.200500461>

- 4) Kulkarni, A.P.; Tonzola, C.J.; Babel, A.; Jenekhe, S.A. Electron Transport Materials for Organic Light-Emitting Diodes. *Chem. Mater.* **2004**, 16, 4556-4573. <https://doi.org/10.1021/cm0494731>
- 5) Hameed, S.; Predeep, P.; Baiju, M.R. Polymer Light Emitting Diodes-a Review on Materials and Techniques. *Rev. Adv. Mater. Sci.* **2010**, 26, 30-42.
- 6) Gross, M.; Muller, D.C.; Nothofer, H.G.; Scherf, U.; Neher, D.; Brauchle, C.; Meerholz, K. Improving the Performance of Doped  $\pi$ -conjugated Polymers for use in Organic Light-Emitting Diodes. *Nature.* **2000**, 405 (6787), 661-5. <https://doi.org/10.1038/35015037>
- 7) Rahman, M.D.A.; Kumar, P.; Park, D.S.; Shim, Y.B. Electrochemical Sensors Based on Organic Conjugated Polymers. *Sensors.* **2008**, 8 (1), 118-141. <https://doi.org/10.3390/s8010118>
- 8) Saxena, V.; Aswal, D.K. Conducting Polymers in Sensor Applications (Control, Robotics and amp; Sensors, **2016**). *Organic Sensors: Materials and Applications*, Chapter 1, 1-70. [https://doi.org/10.1049/PBCE100E\\_ch1](https://doi.org/10.1049/PBCE100E_ch1)
- 9) Wang, H.; Barrett, M.; Duane, B.; Gu, J.; Zenhausern, F. Materials and Processing of Polymer-Based Electrochromic Devices. *Materials Science and Engineering: B.* **2018**, 228, 167-174. <https://doi.org/10.1016/j.mseb.2017.11.016>
- 10) Keersmaecker, M.D.; Lang, A.W.; Österholm, A.M.; Reynolds, J.R. All Polymer Solution Processed Electrochemical Devices: A Future without Indium Tin Oxide? *ACS Appl. Mater.Interfaces.* **2018**, 10 (37), 31568-31579. <https://doi.org/10.1021/acsami.8b10589>
- 11) Neo, W.T.; Ye, Q.; Chua, S.J.; Xu, J. Conjugated Polymer-Based Electrochromics: Materials, Device Fabrication and Application Prospects. *Journal of Materials Chemistry C.* **2016**, 4, 7364-7376. <https://doi.org/10.1039/C6T01150K>

- 12) DiCarmino, P.M.; Schon, T.B.; McCormick, T.M.; Klein, P.P.; Seferos, D.S. Donor-Acceptor Polymers for Electrochemical Supercapacitors: Synthesis, Testing, and Theory. *J. Phys. Chem. C*. **2014**, 118 (16), 8295-8307. <https://doi.org/10.1021/jp5016214>
- 13) Mike, J.F.; Lutkenhaus, J.L. Recent Advances in Conjugated Polymer Energy Storage. *Journal of Polymer Science, B: Polymer Physics*. 2013. 51, 468-480. <https://doi.org/10.1002/polb.23256>
- 14) Chen, Y.J.; Yang, S.H.; Hsu, C.S. Synthesis of Conjugated Polymers for Organic Solar Cell Applications. *Chem. Rev.* **2009**. 109 (11), 5868-5923. <https://doi.org/10.1021/cr900182s>
- 15) Xia, D.; Li, C.; Li, W. Crystalline Conjugated Polymers for Organic Solar Cells: From Donor, Acceptor to Single-Component. *Chem. Rec.* **2019**, 19, 962-972. <https://doi.org/10.1002/tcr.201800131>
- 16) Kruželák, J.; Kvasnicáková, A.; Hložeková, K.; Hudec, I. Progress in Polymers and Polymer Composites used as Efficient Materials for EMI Shielding. *Nanoscale Adv.* **2021**, 3, 123-172. <https://doi.org/10.1039/D0NA00760A>
- 17) Liu, C.; Wang, L.; Liu, S.; Tong, L.; Liu, X. Fabrication Strategies of Polymer-Based Electromagnetic Interference Shielding Materials. *Advanced Industrial and Engineering Polymer Research*. **2020**, 3 (4), 149-159. <https://doi.org/10.1016/j.aiepr.2020.10.002>
- 18) Li, B.; Santhanam, S.; Schultz, L.; Jeffries-El, M.; Ioyu, M.C.; Sauv e, G.; Cooper, J.; Zhang, R.; Revelli, J.C.; Kusne, A.G.; Snyder, J.L.; Kowalewski, T.; Weiss, L.E.; McCullough, R.D.; Fedder, G.K.; Lambeth, D.N. Inkjet Printed Chemical Sensor Array Based on Polythiophene Conductive Polymers. *Sensors and Actuators, B*. **2007**, 123, 651-660. <https://doi.org/10.1016/j.snb.2006.09.064>

- 19) Finn, P.A.; Jacobs, I.E.; Armitage, A.; Wu, R.; Paulsen, B.D.; Freeley, M.; Palma, M.; Rivnay, J.; Siringhaus, H.; Nielsen, C.B. Effect of Polar Side Chains on Neutral and p-Doped Polythiophene. *J. Mater. Chem. C.*, 2020, 8, 16216-16223. <https://doi.org/10.1039/D0TC04290K>
- 20) Chae, H.; Han, J.M.; Ahn, Y.; Kwon, J.E.; Lee, W.H.; Kim, B.G. NO<sub>2</sub>-Affinitive Amorphous Conjugated Polymer for Field-Effect Transistor Sensor Toward Improved NO<sub>2</sub> Detection Capability. *Adv. Mater. Technol.* 2020, 6, 2100580. <https://doi.org/10.1002/admt.202100580>.
- 21) Lipatov, A.; Varezchnikov, A.; Wilson, A.P.; Sysoev, V.; Kolmakov, A.; Sinitskii, A. Highly Selective Gas Sensor Arrays Based on Thermally Reduced Graphene Oxide. *Nanoscale*. **2013**, 5, 5426-5434. <https://doi.org/10.1039/C3NR00747B>
- 22) Alzate-Carvajal, N.; Luican-Mayer, A. Functionalizing Graphene Surfaces for Selective Gas Sensing. *ACS Omega*. **2020**, 5 (34), 21320-21329. <https://doi.org/10.1021/acsomega.0c02861>
- 23) Majhi, S.M.; Mirzaei, A.; Kim, H.W.; Kim, S.S. Reduced Graphene Oxide (rGO)-Loaded Metal-Oxide Nanofiber Gas Sensors: an Overview. *Sensors*. **2021**, 21 (4), 1352. <https://doi.org/10.3390/s21041352>
- 24) Guo, L.; Hao, Y.W.; Li, P.L.; Song, J.F.; Yang, R.Z.; Fu, X.Y.; Xie, S.Y.; Zhao, J.; Zhang, Y.L. Improved NO<sub>2</sub> Gas Sensing Properties of Graphene Oxide Reduced by Two-Beam-Laser-Interference. *Scientific Reports*. **2018**, 8: 4918. <https://doi.org/10.1038/s41598-018-23091-1>
- 25) Yang, M.; Wang, Y.; Dong, L.; Xu, Z.; Liu, Y.; Hu, N.; Kong, E.S.W.; Zhao, J.; Peng, C. Gas Sensors Based on Chemically Reduced Holey Graphene Oxide Thin Films. *Nanoscale Research Letters*. **2019**, 14, 218. <https://doi.org/10.1186/s11671-019-3060-5>
- 26) Joshi, N.; Hayasaka, T.; Liu, Y.; Liu, H.; Oliveira Jr., O.N.; Lin, L. A Review on Chemiresistive Room Temperature Gas Sensors Based on Metal Oxide Nanostructures, graphene and 2D

Transition Metal Dichalcogenides. *Microchimica Acta*. **2018**, 185, 213.

<https://doi.org/10.1007/s00604-018-2750-5>

27) Zulaikha, S.; Demon, N.; Kamisan, A.I.; Abdullah, N.; Aminah, N.N.; Khim, O.K.; Kasim,

N.Z.M.; Yahya, M.Z.A.; Manaf, N.A.A.M.; Azmi, A.F.M.; Halim, N.A. Graphene-Based

Materials in Gas Sensor Applications: A Review. *Sensors and Materials*. **2020**, 32 (2), 759-777.

<https://doi.org/10.18494/SAM.2020.2492>

28) Basu, S.; Bhattacharyya, P. Recent Developments on Graphene and Graphene Oxide Based Solid

State Gas Sensors. *Sensors and Actuators B: Chemical*. **2012**, 173, 1-21.

<https://doi.org/10.1016/j.snb.2012.07.092>

29) Han, T.; Gao, S.; Wang, Z.; Fei, T.; Liu, S.; Zhang, T. Investigation of the Effect of Oxygen-

Containing Groups on Reduced Graphene Oxide-Based Room-Temperature NO<sub>2</sub> Sensor. *Journal*

*of Alloys and Compounds*. **2019**, 801, 142-150. <https://doi.org/10.1016/j.jallcom.2019.06.125>

30) Zhang, Z.; Zhang, X.; Luo, W.; Yang, H.; He, Y.; Liu, Y.; Zhang, X.; Peng, G. Study on

Adsorption and Desorption of Ammonia on Graphene. *Nanoscale Research Letters*. **2015**, 10,

359. <https://doi.org/10.1186/s11671-015-1060-7>

31) Peng, Y.; Li, J. Ammonia Adsorption on Graphene and Graphene Oxide: a First-Principles

Study. *Frontiers of Environmental Science and Engineering*. **2013**, 7, 403-411.

<https://doi.org/10.1007/s11783-013-0491-6>

32) Tang, S.; Cao, Z. Adsorption and Dissociation of Ammonia on Graphene Oxides: a First-

Principles Study. *J. Phys. Chem. C*. **2012**, 116 (15), 8778-8791.

<https://doi.org/10.1021/jp12218w>

- 33) Kang, Y.; Kwak, D.H.; Kwon, J.E.; Kim, B.G.; Lee, W.H. NO<sub>2</sub>-Affinitive Conjugated Polymer for Selective Sub-Parts-Per-Billion NO<sub>2</sub> Detection in a Field-Effect Transistor Sensor. *ACS Appl. Mater. Interfaces*. **2021**, 13(27), 3190-31918 <https://doi.org/10.1021/acsami.1c05681>
- 34) Procek, M.; Kepska, K.; Stolarczyk, A. A Study on the Impact of Poly(3-Hexylthiophene) Chain Length and Other Applied Side-Chains on the NO<sub>2</sub> Sensing Properties of Conducting Graft Copolymers. *Sensors (Basel)*. **2018**, 18(3): 928. <https://doi.org/10.3390/s18030928>.
- 35) Maciak, E.; Procek, M.; Kepska, K.; Stolarczyk, A. Study of Optical and Electrical Properties of Thin Films of the Conducting Comb-like Graft Copolymer of Polymethylsiloxane with Poly(3-Hexylthiophene) and Poly(ethylene) Glycol Side Chains for Low Temperature NO<sub>2</sub> Sensing. *Thin Solid Films Part B*. 2016, 618, 277-285. <https://doi.org/10.1016/j.tsf.2016.08.031>
- 36) Wagner, J.; Jang, H.J.; Han, J.; Katz, H.E. Enhanced and Unconventional Responses in Chemiresistive Sensing Devices for Nitrogen Dioxide and Ammonia from Carboxylated Alkylthiophene Polymers. *Mater. Horiz.* **2020**, 7, 1358-1371. <https://doi.org/10.1039/D0MH00049C>
- 37) Amna, B.; Siddiqi, H.M.; Hassan, A.; Ozturk, T. Recent Developments in the Synthesis of Regioregular Thiophene-Based Conjugated Polymers for Electronic and Optoelectronic Applications using Nickel and Palladium-Based Catalytic Systems. *RSC Adv.* **2020**, 10, 4322-4396. <https://doi.org/10.1039/C9RA09712K>
- 38) Yokoyama, A.; Miyakoshi, R.; Yokozawa, T. Chain-Growth Polymerization for Poly(3-hexylthiophene) with a Defined Molecular Weight and Low Polydispersity. *Macromolecules*. **2004**, 37 (4), 1169-1171. <https://doi.org/10.1021/ma035396o>

- 39) Kiriv, A.; Senkovskyy, V.; Sommer, M. Kumada Catalyst-Transfer Polycondensation: Mechanism, Opportunities, and Challenges. *Macromol. Rapid. Commun.* **2011**, *32*, 1503-1517. <https://doi.org/10.1002/marc.201100316>.
- 40) Verheven, L.; Levsen, P.; Van Den Eede, M.P.; Ceunen, W.; Hardeman, T.; Koeckelberghs, G. Advances in the Controlled Polymerization of Conjugated Polymers. *Polymer.* **2017**, *108*, 521-546. <https://doi.org/10.1016/j.polymer.2016.09.085>
- 41) Stefan, M.C.; Javier, A.E.; Osaka, I.; McCullough, R.D. Grignard Metathesis Method (GRIM): Toward a Universal Method for the Synthesis of Conjugated Polymers. *Macromolecules.* **2009**, *42*, 30-32. <https://doi.org/10.1021/ma8020823>
- 42) Sheina, E.E.; Kheronsky, S.M.; Jones, E.G.; McCullough, R.D. Highly Conductive, Regioregular Alkoxy-Functionalized Polythiophenes: a New Class of Stable Low Band Gap Materials. *Chem. Mater.* **2005**, *17* (13), 3317-3319. <https://doi.org/10.1021/cm050083o>
- 43) Dong, B.X.; Nowak, C.; Onorato, J.W.; Ma, T.; Niklas, J.; Poluektov, O.G.; Grocke, G.; DiTusa, M.F.; Escobedo, F.A.; Luscombe, C.K.; Nealey, P.F.; Patel, S.N. Complex Relationship Between Side-Chain Polarity, Conductivity, and Thermal Stability in Molecularly Doped Conjugated Polymers. *Chem. Mater.* **2021**, *33*, 741-573. <https://doi.org/10.1021/acs.chemmater.0c04153>
- 44) Bauerle, P.; Scheib, S. Synthesis and Characterization of Thiophenes, Oligothiophenes, and Polythiophenes with Crown Ether Units in Direct  $\pi$ -Conjugation. *Acad. Polymer.* **1995**, *46*, 124-129. <https://doi.org/10.1002/actp.1995.010460204>
- 45) Zong, K.; Madrial, L.; Groenendaal, L.B.; Reynolds, J.R. 3,4-Alkylenedioxy Ring Formation via Double Mitsunobu Reactions: An Efficient Route for the Synthesis of 3,4-Ehtylenedioxythiophene (EDOT) and 3,4-Propylenedioxythiophene (ProDOT) Derivatives as

Monomers for Electron-Rich Conducting Polymers. *Chem. Communications*. **2002**, 2498-2499.

<https://doi.org/10.1039/B205907J>

- 46) Fan, H.; Li, H.; Han, J.; McKeever, N.; Yu, J.; Katz, H.E. A Humid-Air-Operable, Now-Responsive Polymer Transistor Series Circuit with Improved Signal-to-Drift Ratio Based on Polymer Semiconductor Oxidation. *ACS Sens.*, 2019, 4(12), 3240-3247.

<https://doi.org/10.1021/acssensors.9b01751>

- 47) Chu, Y.; Li, H.; Huang, J.; Katz, H.E. High Signal-to-Noise Chemical Sensors Based on Compensated Organic Transistor Circuits. *Adv. Mater. Technol.* 2019, 4, 1900410.

<https://doi.org/10.1002/admt.201900410>.

- 48) Han, S.; Yang, Z.; Li, Z.; Zhuang, X.; Akinwande, D.; Yu, J. Improved Room Temperature NO<sub>2</sub> Sensing Performance of Organic Field-Effect Transistor by Directly Blending a Hole-Transporting/Electron-Blocking Polymer into the Active Layer. *ACS Appl. Mater. Interfaces*.

**2018**, 10, 38280-38286. <https://doi.org/10.1021/acsami.8b07838>

- 49) Callari, M.R.; Izquierdo, J.E.E.; Braga, G.S.; Dirani, E.A.T.; Pereira-da-Silva, M.A.; Rodriguez, E.F.G.; Fonseca, F.J. Enhanced Sensitivity of Gas Sensor Based on Poly(3-hexylthiophene) Thin Film Transistors for Disease Diagnosis and Environment Monitoring. *Sensors*. **2015**, 15, 9592-

9609. <https://doi.org/10.3390/s150409592>

- 50) Roisin, P.; Wright, J.D.; Nolte, R.J.M.; Sielcken, O.E.; Thorpe, S.C. Gas-Sensing Properties of Semiconducting Films of Crown-Ether-Substituted Phthalocyanines. *J.Mater.Chem.* 1992, 2,

131-137. <https://doi.org/10.1039/JM9920200131>

- 51) Patil, A.O.; Ikenoue, Y.; Basescu, N.; Colaneri, N.; Chen, J.; Wudl, F.; Heeger, A.J. Self-doped conducting polymers. *Synthetic Metals*. **1987**, 20 (2), 151-159. [https://doi.org/10.1016/0379-6779\(87\)90554-6](https://doi.org/10.1016/0379-6779(87)90554-6)
- 52) Yano, H.; Kudo, K.; Marumo, K.; Okuzaki, H. Fully soluble self-doped poly(3,4-ethylenedioxythiophene) with an electrical conductivity greater than 1000 S cm<sup>-1</sup>. *Science Advances*. **2019**, 5 (4), eaav9492. <https://doi.org/10.1126/sciadv.aav9492>
- 53) Li, X.; An, H.; Strzalka, J.; Lutkenhaus, J.; Verduzco, R. Self-Doped conjugated polymeric binders improve the capacity and mechanical properties of V<sub>2</sub>O<sub>5</sub> cathodes. *Polymers*. **2019**, 11 (4): 589. <https://doi.org/10.3390/polym11040589>
- 54) Jang, H.J.; Wagner, J.; Li, H.; Zhang, Q.; Mukhopadhyaya, T.; Katz, H.E. Analytical Platform to Characterize Dopant Solution Concentrations, Charge Carrier Densities in Films and Interfaces, and Physical Diffusion in Polymers Utilizing Remote Field-Effect Transistors. *J. Am. Chem. Soc.* **2019**, 141 (12), 4861-4869. <https://doi.org/10.1021/jacs.8b13026>
- 55) Cavallari, M.R., Izquierdo, J.E.E., Braga, G.S., Dirani, E.A.T., Pereira-da-Silva, M.A., Rodríguez, E.F.G., Fonseca, F.J. Enhanced Sensitivity of Gas Sensor Based on Poly(3-hexylthiophene) Thin-Film Transistors for Disease Diagnosis and Environment Monitoring. *Sensors*, **2015**, 15, 9592-9609. <https://doi.org/10.3390/s150409592>.
- 56) Kim, K.H., Jahan, S.A., Kabir, E. A Review of Breath Analysis for Diagnosis of Human Health. *TrAC Trends Anal. Chem.* **2012**, 33,1-8. <https://doi.org/10.1016/j.trac.2011.09.013>
- 57) Ruzsányi, V., Kalapos, M.P. Breath Acetone as a Potential Marker in Clinical Practice. *J. Breath Res.* **2017**, 11, 024002. <https://doi.org/10.1088/1752-7163/aa66d3>.

- 58) Bertoni, C., Naclerio, P., Viviani, E., Dal Zilio, S., Carrato, S., Fraleoni-Morgera, A.  
Nanostructured P3HT as a Promising Sensing Element for Real-Time, Dynamic Detection of  
Gaseous Acetone. *Sensors*, **2019**, 1296. <https://doi.org/10.3390/s19061296>.
- 59) Itoh, T., Koyama, Y., Shin, W., Akamatsu, T., Tsuruta, A., Masuda, Y., Uchiyama, K. Selective  
Detection of Target Volatile Organic Compounds in Contaminated Air Using Sensor Array with  
Machine Learning: Aging Notes and Mold Smells in Simulated Automobile Interior  
Contaminant Gases. *Sensors*, **2020**, 20(9), 2687. <https://doi.org/10.3390/s20092687>.
- 60) Bishop, C.M. (2006). *Pattern Recognition and Machine Learning*. Springer; New York, NY.